—Technical Paper—

Oxygen Chemical Diffusion at $LaMnO_3$ Film/YSZ under Cathodic Polarization by Secondary Ion Mass Spectrometry

Teruhisa HORITA,* Katsuhiko YAMAJI, Hideyuki NEGISHI, Natsuko SAKAI, and Harumi YOKOKAWA

National Institute of Materials and Chemical Research (NIMC) (Higashi 1-1, Tsukuba, Ibaraki 305-8565, Japan)

Received November 26, 1999 ; Accepted January 11, 2000

Oxygen chemical diffusion at $La_{0.92}MnO_3$ film/YSZ interface was investigated under cathodic polarized condition. Secondary ion mass spectrometry (SIMS) analysis was performed for the samples with isotope oxygen exchange (^{16}O /^{18}O exchange at 1073 K). The diffusion profiles of ^{18}O in the $La_{0.92}MnO_3$ film showed that fast ^{18}O diffusion under cathodic polarization. The active sites for oxygen incorporation were distributed in many spots on YSZ single crystal surface from the SIMS imaging analysis. Also, Mn diffusion from $LaMnO_3$ to YSZ was observed in many spots on YSZ surface. Oxygen permeation current density through the $La_{0.92}MnO_3$ film was calculated by the defect model of $LaMnO_3$ under cathodic polarization, which was a smaller than the observed value.

Key Words : Oxygen Chemical Diffusion, $LaMnO_3$, Cathodic Polarization, Secondary Ion Mass Spectrometry

1 Introduction

Doped $LaMnO_3$ has been considered as a cathode for solid oxide fuel cells (SOFCs) because of its relatively high electronic conductivity and high catalytic activity for oxygen reduction.[1] At the interface of O_2/doped $LaMnO_3$/Y_2O_3-stabilized ZrO_2 (YSZ) (Three Phase Boundary, TPB), oxygen molecules can be reduced to oxide ions (O^{2-}), and they are transported into the anode side via the electrolyte.[2-5] Recently, we have demonstrated the application of secondary ion mass spectrometry (SIMS) technique to analyze the distribution of active sites for oxygen incorporation/reduction at $La_{0.9}Sr_{0.1}MnO_3$/YSZ interface.[6,7] In our previous study, the TPB was found to be the main reaction sites for oxygen reduction. In addition, oxide ion (O^{2-}) diffusion was observed in the dense $La_{0.9}Sr_{0.1}MnO_3$. Figure 1 shows one example of our SIMS images (Fig.1(a) & (b))[6] and schematic diagram of oxide ion diffusion at the interface (Fig.1(c)). A mesh shaped dense $La_{0.9}Sr_{0.1}MnO_3$ layer was fabricated on the YSZ substrate, and a stable isotope of oxygen ($^{18}O_2$) was adopted as a diffusion marker. In the SIMS images of $^{18}O^-$ on the $La_{0.9}Sr_{0.1}MnO_3$ mesh/YSZ surface (Fig.1(a)), the higher concentration of $^{18}O^-$ is observed in the whiter color at the $La_{0.9}Sr_{0.1}MnO_3$ mesh part. This indicates that the surface of $La_{0.9}Sr_{0.1}MnO_3$ is active for oxygen exchange than that of YSZ. In the $^{18}O^-$ image of YSZ surface after removing the $La_{0.9}Sr_{0.1}MnO_3$ mesh (Fig.1(b)), the higher $^{18}O^-$ concentration parts are shown in the shape of the mesh. That is, ^{18}O can diffuse through the $La_{0.9}Sr_{0.1}MnO_3$ mesh via the interface of $La_{0.9}Sr_{0.1}MnO_3$/YSZ. The diffusion distance of ^{18}O under non-polarized condition was estimated to be about 350 nm, which was too short to diffuse through the $La_{0.9}Sr_{0.1}MnO_3$ mesh (width: 1920 nm, thickness: 490 nm) in the $^{16}O/^{18}O$ exchange condition ($^{16}O/^{18}O$ exchange for 600 s at 973 K).[6] Therefore, cathodic polarization could enhance the diffusion of ^{18}O in the $La_{0.9}Sr_{0.1}MnO_3$ mesh. Also, some high spots of $^{18}O^-$ are observed in the center part of the mesh. This indicates that the active sites for oxygen incorporation are not all the interface of $La_{0.9}Sr_{0.1}MnO_3$ mesh/YSZ. Since the YSZ substrate was a polycrystal-sintered disk, grain boundaries and small pores on the surface could affect the oxygen incorporation.

The possibility of oxygen chemical diffusion in $LaMnO_3$ has been already suggested, and the electrochemical properties of $LaMnO_3$ film have been reported by several authors.[8-15] However, still some unclear points have left about the oxygen chemical diffusion in $LaMnO_3$ under cathodic polarization. If the movements of

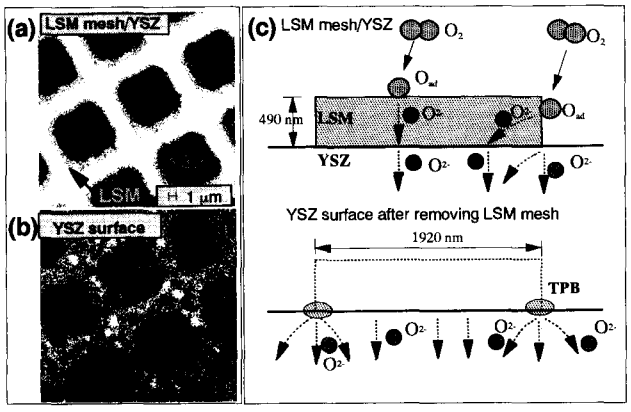

Fig. 1 SIMS images of $^{18}O^-$ at $La_{0.9}Sr_{0.1}MnO_3$(LSM) mesh/YSZ interface(a) and YSZ surface (b), and schematic diagram for oxygen transport at $La_{0.9}Sr_{0.1}MnO_3$(LSM) mesh/YSZ interface (c). The upper part of Fig. 1(c) indicates the schematic diagram of O^{2-} diffusion at the LSM mesh/YSZ interface. The lower part of Fig. 1(c) indicates the O^{2-} diffusion in YSZ.

oxygen/oxide ions in $LaMnO_3$ can be observed directly, it will give us a valuable information. The aim of this study is to elucidate the chemical diffusion of oxygen at the dense $LaMnO_3$ film/YSZ interface by SIMS analysis for $^{16}O/^{18}O$ exchanged samples under cathodic polarization, and to estimate the chemical diffusion of oxygen by calculation. To reduce the reaction between $LaMnO_3$ and YSZ, A-site deficient $LaMnO_3$ ($La_{0.92}MnO_3$) was adopted as a cathode film. Also, to eliminate the effect of grain boundaries and pores, a single crystal YSZ was adopted as a substrate.

2 Experimental

2. 1 Samples

$La_{0.92}MnO_3$ powders were prepared by mixing an appropriate $La(NO_3)_3$ and $Mn(NO_3)_3$ solutions, and co-precipitated into oxalates in the oxalic acid solution. The co-precipitated oxalates were dried at 673 K in air and fired at 1273 K for 5 h in air. The $La_{0.92}MnO_3$ powders obtained were confirmed to have no impurities by X-ray powder diffraction. A Y_2O_3 stabilized ZrO_2 single crystal (8 mol% Y_2O_3 substituted) was used as a substrate (Earth Chemical Co. Ltd., Japan, YSZ) to eliminate the effect of grain boundary and pores. The surface of the YSZ single crystal ((100) oriented plane) was smooth enough (less than 5 nm of 凸凹), and no pores and grain boundaries were observed on the surface by atomic force microscope (AFM) before and after $LaMnO_3$ film application on YSZ single crystal. A dense $La_{0.92}MnO_3$ film was fabricated by RF-sputtering method with a thickness of 0.49 μm on a single crystal YSZ. During sputtering, the substrate was heated at 973 K in a vacuum condition (pressure around 3×10^{-8} bar). The $La_{0.92}MnO_3$ film/YSZ samples were healed at 1273 K in air to attach the Pt-reference and Pt-counter electrode.

2. 2 Isotopic oxygen exchange ($^{16}O/^{18}O$ exchange) under cathodic polarization

Fig. 2 shows schematic diagram of isotopic oxygen exchange ($^{16}O/^{18}O$ exchange) under cathodic polarization: Fig. 2(a) shows schematic diagram of $^{16}O/^{18}O$ exchange system and Fig. 2(b) shows schematic diagram of cathodic polarization set up. Samples of $La_{0.92}MnO_3$ film/YSZ were initially annealed at 1073 K in $^{16}O_2$ atmosphere to saturate ^{16}O in the sample (Fig.2(a)). After annealing in $^{16}O_2$ under cathodic polarization, the atmosphere was quickly switched to $^{18}O_2$ at the same oxygen partial pressure of 0.08 bar (The concentration of $^{18}O_2$ was 96 vol%). The concentration of each isotope oxygen ($^{16}O_2$ and $^{18}O_2$) in the gas phase during $^{16}O/^{18}O$ exchange was measured by gas monitor (Massmate-300, Ulvac Co.) with sampling a small amount of gas. Because the gas volume of $^{18}O_2$ was sufficiently large enough compared with that of $^{16}O_2$ emitted from the sample, the concentration of ^{18}O in the gas phase is thought to be constant during $^{16}O/^{18}O$ exchange. The $^{16}O/^{18}O$ exchange duration was 600 s, and the sample was quenched from 1073 K to 298 K within 30 s by N_2 flow. The applied voltage at $La_{0.92}MnO_3$ film/YSZ was about -0.5 V against the reference electrode (this gives the cathodic polarization of $\eta = -0.45$ V versus air). The current-voltage characteristics of this sample was measured in the oxygen partial pressure of 0.08 bar at 1073 K before $^{16}O/^{18}O$ exchange.

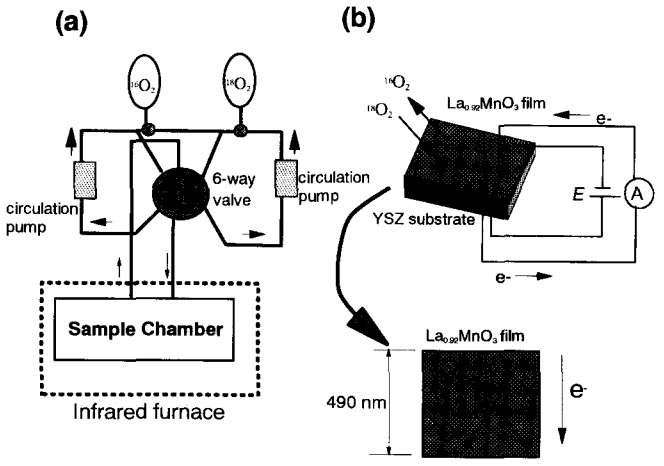

Fig. 2 Schematic diagram of isotope oxygen exchange (a) and sample setup for cathodic polarization (b). The lower part of Fig. 2(b) shows schematic diagram of O^{2-} and $V_O^{\cdot\cdot}$ diffusion in $La_{0.92}MnO_3$ film under current flow.

2. 3 SIMS analysis

After $^{16}O/^{18}O$ exchange, the samples were analyzed by secondary ion mass spectrometry (SIMS, ims-5 f, CAMECA) in its depth or imaging analysis mode. In the depth analysis mode, a relatively strong primary Cs^+ beam sputtered the sample surface (*ca.* 30 μm in diameter) in an area of 150×150 μm^2. In the imaging mode, a finely focused primary Cs^+ beam (*ca.* 0.2-0.3 μm in diameter) was scanned on the surface of YSZ with an area of 30×30 μm^2. The measured secondary ions were $^{16}O^-$, $^{18}O^-$, $La^{16}O^-$, $Mn^{16}O^-$, $Y^{16}O^-$, and $Zr^{16}O^-$. Because the coupling ions of metal and $^{16}O^-$ showed high secondary ion intensities under this experimental condition, these secondary ions were measured as a metallic concentration. After SIMS sputtering, the depth of the craters was measured by the surface profiler system (Dektak,[3] Veeco /Sloan Technology, NY, USA).

3 Results and Discussion

3. 1 Polarization curve of $La_{0.92}MnO_3$ film/YSZ

Figure 3 shows cathodic polarization curves of $La_{0.92}MnO_3$ film/YSZ in the oxygen partial pressure of 0.08 bar, before $^{16}O/^{18}O$ exchange. The polarization curve shows hysterisis between forward and backward directions: the higher cathodic polarization currents were observed in the backward polarization direction. This phenomenon was also reported in the previous works for doped-$LaMnO_3$ film electrode.[8-11] The $^{16}O/^{18}O$ exchange was performed at the cathodic polarization of -0.45 V under almost constant current density(5.3 mA cm^{-2}). If the reference electrode (Pt) is in equilibrium with oxygen partial pressure of the ambient atmosphere ($p_1(O_2)$ = 0.08 bar), the cathodic polarization gives the oxygen partial pressure at the interface of $LaMnO_3$/YSZ by the following equation:

$$p_2(O_2) = p_1(O_2)\exp\left(\frac{4F\eta}{RT}\right) \quad (1)$$

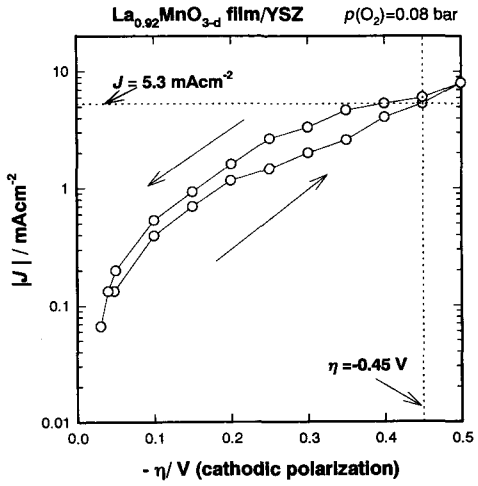

Fig. 3 Cathodic polarization curve of $La_{0.92}MnO_3$ film/YSZ sample (cell temperature at 1073 K, at $p(O_2) = 0.08$ bar).

where $p_2(O_2)$ indicates the oxygen partial pressure at the $LaMnO_3$/YSZ interface, F the Farady constant, η cathodic polarization, R gas constant, and T temperature. The cathodic polarization of -0.45 V reduces the oxygen partial pressure at the $LaMnO_3$ film/YSZ interface of $p_2(O_2) = 2.8 \times 10^{-10}$ bar in this experimental condition.

3. 2 Diffusion profiles of ^{18}O at $La_{0.92}MnO_3$ film/YSZ interface

Figure 4 shows diffusion profiles of ^{18}O around the $La_{0.92}MnO_3$/YSZ interface under non-polarized condition ($\eta = 0$ V) and cathodic polarized condition ($\eta = -0.45$ V). The ^{18}O concentration ratio at the depth of x, $C(x)$, is defined by the following equation:

$$C_{18}(x) = I(^{18}O^-) / \{I(^{18}O^-) + I(^{16}O^-)\} \qquad (2)$$

where $I(^{18}O^-)$ and $I(^{16}O^-)$ indicate the each secondary ion signal counts measured by SIMS, respectively. From the diffusion profiles of ^{18}O under non-polarized condition, the isotope oxygen diffusion coefficient (D) and surface

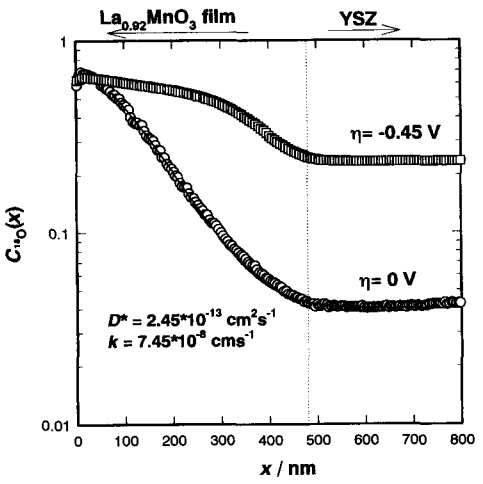

Fig. 4 Diffusion profiles of ^{18}O at $La_{0.92}MnO_3$ film/YSZ interface (○: cathodic polarization at 0 V, □: cathodic polarization at -0.45 V, the $^{16}O/^{18}O$ exchange for 600 s at 1073 K).

oxygen exchange coefficient (k) can be calculated by the following appropriate equation:[16]

$$C(x) = (C_g - C_{bg}) \cdot \left[\mathrm{erfc}\left(\frac{x}{2\sqrt{Dt}}\right) - \exp(hx + h^2Dt)\,\mathrm{erfc}\left(\frac{x}{2\sqrt{Dt}} + hDt\right)\right] + C_{bg} \qquad (3)$$

where, C_g and C_{bg} indicate the isotope oxygen concentration in the gas phase and in $LaMnO_3$ bulk, respectively ($C_g = 0.96$ and $C_{bg} = 0.03$ in this calculation). The "erfc" in eq. (3) indicates the error function. Because ^{18}O can diffuse through the $La_{0.92}MnO_3$ film into the YSZ substrate in this $^{16}O/^{18}O$ exchange condition, C_{bg} was set the value of 0.03 (this is the higher values than the natural abundance level of 0.002). The parameter h is related to D and k ($h = k/D$), and x is depth from the sample surface. The fitting line of the diffusion profile is drawn in the solid line in the figure, which shows a good fit to the measured data. The obtained diffusion coefficient and surface oxygen exchange coefficient are $D = 2.45 \times 10^{-13}$ $cm^2\ s^{-1}$ and $k = 7.45 \times 10^{-8}$ $cm^2\ s^{-1}$, respectively. These values are almost consistent with the reported data for the bulk of $LaMnO_3$.[15] For the diffusion profile of ^{18}O under cathodic polarization at -0.45 V, the diffusion profile shows relatively flat in the $La_{0.92}MnO_3$ film and some decrease of ^{18}O concentration with a steep slope around the $La_{0.92}MnO_3$/YSZ interface. The important features of these diffusion profiles are summarized in the following two points, according to the surface region and the inside of $La_{0.92}MnO_3$ film: 1) Concentrations of ^{18}O at the surface for two diffusion profiles are almost same values. This indicates that the surface oxygen exchange rates of $La_{0.92}MnO_3$ film are almost constant regardless the polarization. A small difference for the concentration of ^{18}O under polarization at the surface can be due to extremely high D values versus k value under polarization. 2) A relatively flat diffusion profile of ^{18}O inside the $La_{0.92}MnO_3$ film indicates high diffusivity of ^{18}O in the film under cathodic polarization. Small drop of ^{18}O concentration is observed in the profile around the $La_{0.92}MnO_3$/YSZ interface at a depth of 350-450 nm. This drop can indicate the diffusion of ^{18}O by the concentration difference of ^{18}O in the $La_{0.92}MnO_3$ film, or the existence of obstruction for ^{18}O diffusion around the interface. Experiments for another cathodic polarization voltage are now under examination. The precise analysis will be made in the near future.

3. 3 Distribution of oxygen incorporation at $La_{0.92}MnO_3$ film/YSZ interface

In order to clarify the distribution of oxygen incorporation at the interface of $La_{0.92}MnO_3$ film/YSZ, the surface $La_{0.92}MnO_3$ film was removed by dissolving into HCl solution. After removing the covered $La_{0.92}MnO_3$ film, SIMS imaging analysis was conducted on YSZ surface. Figure 5 shows SIMS images of YSZ surface after removing the $LaMnO_3$ film. The secondary ion images show the distribution of each secondary ion on YSZ surface, close to the interface of $La_{0.92}MnO_3$ film/YSZ. The higher concentration of secondary ions show in the whiter image in

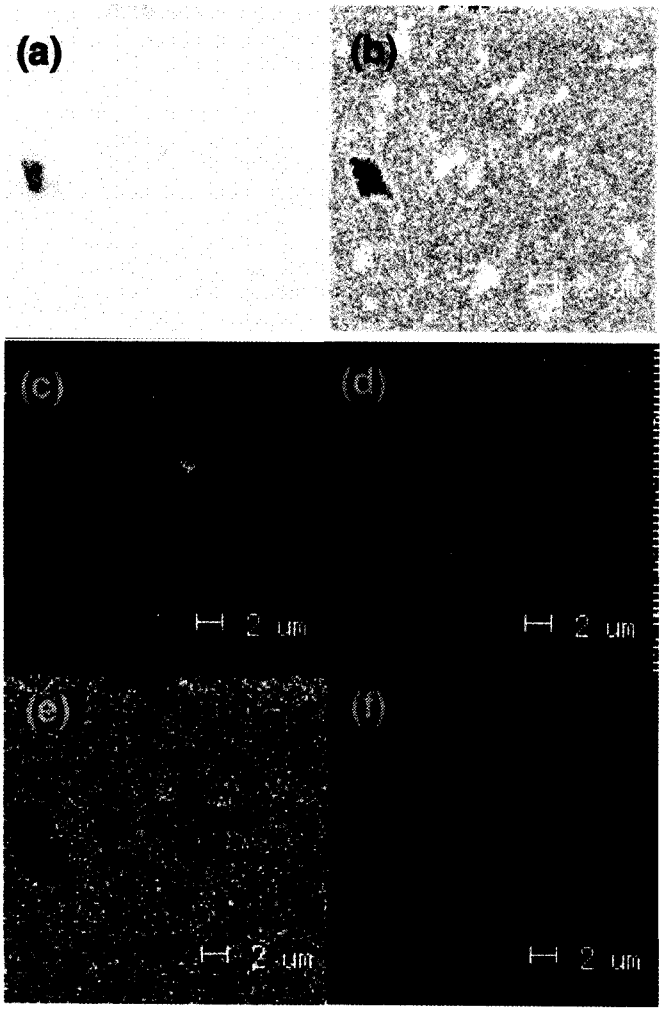

Fig. 5 SIMS images of YSZ single crystal surface after removing the $La_{0.92}MnO_3$ film. (a): $^{16}O^-$, (b): $^{18}O^-$, (c): $Mn^{16}O^-$, (d): $Y^{16}O^-$, (e): $Zr^{16}O^-$, (f): $La^{16}O^-$.

these figures. In Fig. 5(b), spots of high $^{18}O^-$ concentration (about 0.5-2 μm in diameter) are observed on YSZ surface, while no $^{16}O^-$ distribution is observed in Fig.5(a). Therefore, $^{18}O^-$ image can indicate the active sites distribution for oxygen incorporation on YSZ surface. Another interesting feature of this image is the distribution of $Mn^{16}O^-$. Many spots of $Mn^{16}O^-$ indicate the Mn interdiffusion from $LaMnO_3$ to YSZ. During annealing the samples, some amounts of Mn can diffuse into YSZ and can affect the interface properties for oxygen diffusion. In addition, we have already observed the morphological change of the interface during annealing.[17] There is another possibility of morphological change of the YSZ surface, due to the strain during the preparation of smooth surface. The morphological change of the YSZ interface also must be taken into account for precise analysis during the preparation and annealing or current flow experiments. The distribution of $Y^{16}O^-$ and $Zr^{16}O^-$ show almost homogeneous without any significant concentration differences at the surface (Fig. 5(d) & (e)). The image of $La^{16}O^-$ shows almost no count intensity due to low concentration of La on the YSZ surface (Fig.5(f)).

3. 4 Calculation of oxygen permeation through $LaMnO_3$ film under cathodic polarization

For analyzing the oxygen chemical diffusion (oxygen permeation) at the $La_{0.92}MnO_3$ film/YSZ interface, it is important to estimate the concentration of oxygen vacancy ($[V_O^{\cdot\cdot}]$) and the flux of oxide ion($J(O^{2-})$) during cathodic polarization. In the $La_{0.92}MnO_3$ film/YSZ sample, the electron movements can be blocked by the YSZ substrate because YSZ is almost purely oxide ion conductor. When the voltage is applied to the $LaMnO_3$ film/YSZ sample in the cathodic polarized direction, only oxide ions can pass through the $LaMnO_3$ film from high to low oxygen partial pressure (Fig.2(b)). The driving force for oxygen chemical diffusion is the gradient of chemical potential of oxygen, which is attained by the applied voltage. Diffusion of oxide ion through the dense $LaMnO_3$ is considered to occur via oxygen vacancies. So far, some authors have proposed the diffusion model of oxygen in $LaMnO_3$ via the oxygen vacancies.[12-14] In this study, the neutral cluster formation model has been adopted for the calculation of oxygen vacancy concentration.[12] That is, oxygen vacancies are formed accompanying with the Mn^{2+} cluster, Mn_{Mn}'-$V_O^{\cdot\cdot}$-Mn_{Mn}'. The formation of this cluster is written in the following equation by using the Kröger-Vink notation:

$$2Mn_{Mn}^{\times} + O_O^{\times} \longleftrightarrow \langle Mn'_{Mn} - V_O^{\cdot\cdot} - Mn'_{Mn} \rangle + \frac{1}{2}O_2 \quad (4)$$

where, $Mn^{\times}_{Mn}$ and $O^{\times}_{O}$ indicate Mn^{3+} and O^{2-} in the normal position of the lattice of $LaMnO_3$ perovskite, respectively. Mn'_{Mn} and $V_O^{\cdot\cdot}$ indicate the Mn^{2+} and vacancy of oxygen in the lattice, respectively.
The equilibrium constant of this equation is written as,

$$K_4 = \frac{[<Mn'_{Mn} - V_O^{\cdot\cdot} - Mn'_{Mn}>]p(O_2)^{1/2}}{[Mn^{\times}_{Mn}]^2[O^{\times}_{O}]} \quad (5)$$

The electroneutrality condition (eq.(6)) and site relations (eqs.(7) and (8)) are expressed in the followings:

$$2[V_O^{\cdot\cdot}] = [Mn'_{Mn}] \quad (6)$$
$$[Mn^{\times}_{Mn}] + [Mn'_{Mn}] = 1 \quad (7)$$
$$[O^{\times}_{O}] + [V_O^{\cdot\cdot}] = 3 \quad (8)$$

Using these relationship, the eq.(5) is rewritten as follows:

$$K_4 = \frac{[V_O^{\cdot\cdot}]p(O_2)^{1/2}}{(1-2[V_O^{\cdot\cdot}])^2 \cdot (3-[V_O^{\cdot\cdot}])} \quad (9)$$

By fitting to the measured number of oxygen,[17] the vacancy concentration can be calculated as a function of oxygen partial pressure. Figure 6 shows oxygen content ($3 \pm \delta$) and vacancy concentration of $LaMnO_3$ as a function of oxygen partial pressure. The equilibrium constant was calculated to be $K_4 = 4.5 \times 10^{-12}$, by the method of least squares fitting. It is well known that $LaMnO_3$ perovskite has excess oxygen in high oxygen partial pressure region. Therefore, the fitting line could not follow the measured values at the higher oxygen partial pressure region. High oxygen number is thought to be compensated by the metal vacancy in $LaMnO_3$, such as V_{La}'''. We assume that only the oxygen vacancy contributes the oxide ion diffusion in $LaMnO_3$, and the chemical diffusion of oxygen is thought to occur via the oxygen vacancies. From the oxygen partial pressure dependence of vacancy concentration ($-1/2$ powers of oxygen partial pressures), we can calculate the ionic conductivity in $LaMnO_3$ as a function of oxygen partial pressure by the Nernst-Einstein relation as follows:

$$\sigma(O^{2-}) = \frac{4F^2[V_O^{\cdot\cdot}]D_v}{RT\,V_m} \quad (10)$$

where, D_v is the oxygen vacancy diffusion coefficient and V_m is the mole volume of $LaMnO_3$.

When the electronic conductivity is much higher than the ionic conductivity, the oxygen permeation flux (oxide ion flux) can be calculated in the following equation:[13]

$$J(O^{2-}) = -\frac{1}{L}\int_{p_1(O_2)}^{p_2(O_2)} \sigma(O^{2-})\frac{RT}{4F} d\ln p(O_2) \quad (11)$$

where, L indicates the thickness of the $LaMnO_3$ film. Figure 7 shows calculated oxygen permeation current in $LaMnO_3$ (oxide ion flux) as a function of oxygen partial pressure at 1073 K (for calculation, $D_v = 1 \times 10^{-6}$ cm^2 s^{-1}, $V_m = 35$ cm^3 mol^{-1} and $L = 500$ nm are used). The cathodic polarization in this study corresponds to the oxygen partial pressure of 2.8×10^{-10} bar, and this oxygen chemical potential gives the oxygen permeation current of 1.1 mA cm^{-2}. The calculated current density is somewhat smaller than the measured one (5.3 mA cm^{-2}) in this polarization. The possible reasons of this difference are in the following two reasons: 1) reaction at the side of $LaMnO_3$ film/YSZ (at the TPB region), and 2) temperature control error of furnace during polarization, because cell temperature is very sensitive to the position in the infrared furnace.

Precisely speaking, D_v should be replaced to the chemical diffusion coefficient of oxygen, D_{chem}, for calculation of oxygen permeation current in this study. The

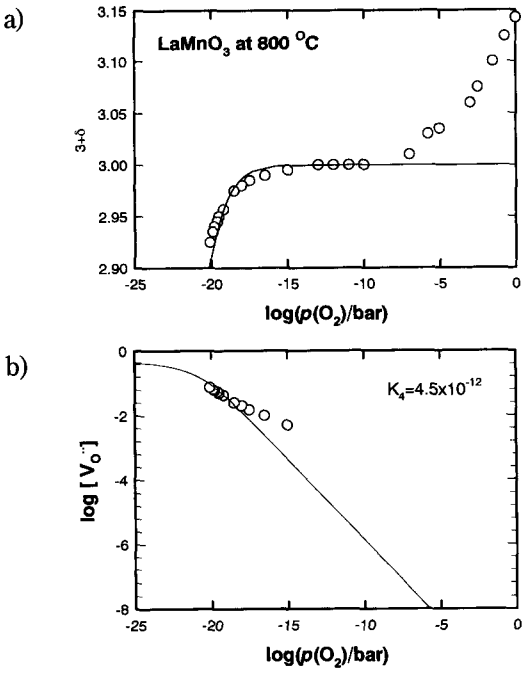

Fig. 6 Oxygen vacancy concentration in $LaMnO_3$ as a function of oxygen partial pressure, (a): number of oxygen ($3 \pm \delta$) in $LaMnO_3$, (b): logarithm of vacancy concentration in $LaMnO_3$ (○: measured values from ref. 18), - - -: fitting line).

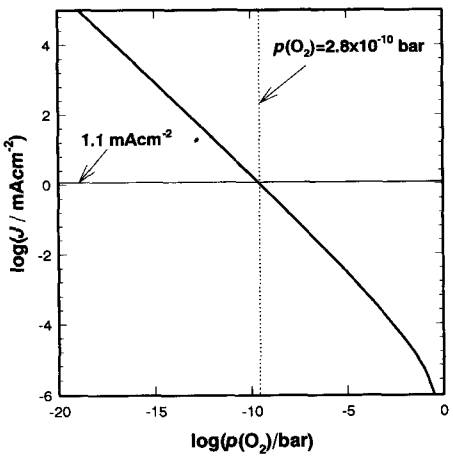

Fig. 7 Oxygen permeation current density ($J(O^{2-})$) in $LaMnO_3$ film as a function of oxygen partial pressure (the thickness of $LaMnO_3$ film is set as 0.5 μm for calculation, at 1073 K).

relationship between D_v and D_{chem} is as follows:

$$D_{chem} = \text{e.f.} * D_v \quad (12)$$

where, e.f. indicates the enhancement factor, which is related to the concentration of oxygen vacancies.[14] From the reference of (14), the e.f. is almost unity in this experimental condition ($p(O_2) > 10^{-10}$ bar, 800℃). Thus, the D_v value is almost same value of D_{chem}.

Here we consider again the diffusion profile of ^{18}O under cathodic polarization at $La_{0.92}MnO_3$ film/YSZ interface (Fig.4). The higher ^{18}O concentration at the $LaMnO_3$ film /YSZ interface can be partly due to the reaction at the TPB under the cathodic polarization of −0.45 V. Diffusion of ^{18}O at the side of the interface can increase the concentration of ^{18}O. However, the flat profile of ^{18}O concentration in the $LaMnO_3$ film indicates the fast chemical diffusion of ^{18}O by cathodic polarization. The analysis of ^{18}O diffusion profile for different cathodic polarization in the $LaMnO_3$ film is under investigation. The effect of cathodic polarization on the ^{18}O diffusion profiles will be reported for the same system in the near future. The concentration drop of ^{18}O around the $La_{0.92}MnO_3$ film/ YSZ interface is considered to be due to two factors: one is the diffusion of Mn from $LaMnO_3$ to YSZ that changes the diffusion property of oxide ions at the interface, the other is the diffusion of ^{18}O by the concentration difference of ^{18}O in the $La_{0.92}MnO_3$ film.

4 Conclusion

Secondary ion mass spectrometry (SIMS) analysis technique determined the diffusion profile of isotope oxygen(^{18}O) and the distribution of active sites for oxygen incorporation at the $La_{0.92}MnO_3$ film/YSZ interface. The cathodic polarization enhanced the chemical diffusion of oxygen through the $La_{0.92}MnO_3$ film by the introduction of oxygen vacancies.

(1) The diffusion profiles of ^{18}O under cathodic polarization were relatively flat in the $La_{0.92}MnO_3$ film, which indicated the fast chemical diffusion of ^{18}O.

(2) The active sites for oxygen incorporation were distributed in many spots on YSZ surface. High concentration spots of Mn were also observed on the surface.

(3) Oxygen permeation current density ($J(O^{2-})$) through the $LaMnO_3$ film was calculated from the defect data of $LaMnO_3$, which was smaller than the observed current density. This can be due to the reaction at the TPB and the interface diffusion of ^{18}O.

Acknowledgements

The authors sincerely thank to Dr. Tohru Kato (Electrotechnical laboratory, ETL) for his preparation of $La_{0.92}$·MnO_3 film on YSZ single crystal. Also, the authors thank to associate professor, Tatsuya Kawada (RISM, Tohoku University) for his valuable discussion about the oxygen permeation in $LaMnO_3$ film.

Part of this study was presented at 6th International Symposium on Solid Oxide Fuel Cells (1999 Joint International Meeting of the Electrochemical Society of Japan and the Electrochemical Society) at Hawaii, October 1999. The corresponding author (T. Horita) thanks to Prof. Dr. E. Ivers-Tiffee and University of Karlsruhe for the support of travel and attendance expenses during the research fellowship of the Alexander von Humboldt Foundation in Germany.

References

1) N. Q. Minh, *J. Am. Ceram. Soc.*, **76**(3), 563 (1993).
2) Y. Takeda, R. Kanno, Y. Tomida, and O. Yamamoto, *J. Electrochem. Soc.*, **134**, 2656 (1987).
3) K. Tsuneyoshi, K. Mori, A.Sawata, J. Mizusaki, and H. Tagawa, *Solid State Ionics*, **35**, 263 (1989).
4) J. Mizusaki, H. Tagawa, K. Tsuneyoshi, and A. Sawata, *J. Electrochem. Soc.*, **138**, 1867 (1991).
5) E. Siebert, A. Hammouche, and M. Kleitz, *Electrochimica Acta*, **40**(11), 1741 (1995).
6) T. Horita, K. Yamaji, M. Ishikawa, N. Sakai, H. Yokokawa, T. Kawada, and T. Kato, *J. Electrochem. Soc.*, **145**(9), 3196 (1998).
7) T. Horita, K. Yamaji, N. Sakai, H. Yokokawa, T. Kawada, and T. Kato, *Solid State Ionics*, **127**, 55 (2000).
8) B. Gharbage, T. Pagnier, and A. Hammou, *J. Electrochem. Soc.*, **141**(8), 2118 (1994).
9) H. Y. Lee, W. S. Cho, S. M. Oh, H. -D. Wiemhöfer, and W. Göpel, *J. Electrochem. Soc.*, **142**(8), 2659 (1995).
10) J. Mizusaki, T. Saito, and H. Tagawa, *J. Electrochem. Soc.*, **143**(10), 3065 (1996).
11) T. Ioroi, T. Hara, Y. Uchimoto, Z. Ogumi, and Z. Takehara, *J. Electrochem. Soc.* **145**(6), 1999 (1998).
12) J. A. van Roosemalen and E. H. P. Cordfunke, *J. Solid State Chemistry*, **93**, 212 (1991).
13) B. A. van Hassel, T. Kawada, N. Sakai, H. Yokokawa, M. Dokiya, and H. J. M. Bouwmeester, *Solid State Ionics*, **66**, 295 (1993).
14) I. Yasuda and M. Hishinuma, *J. Solid State Chemistry*, **123**, 382 (1996).
15) I. Yasuda, K. Ogasawara, M. Hishinuma, T. Kawada, and M. Dokiya, *Solid State Ionics*, **86-88**, 1197 (1996).
16) J. Crank, *The Mathematics of Diffusion*, 2nd Edition, Oxford University Press, Oxford (1975).
17) T. Horita, K. Yamaji, H. Negishi, N. Sakai, H. Yokokawa, and T. Kato, presented at SSI-12 (Thessaloniki, Greece, June 1999), to be published in *Solid State Ionics*.
18) H. Tagawa, N. Mori, H. Takai, Y. Yonemura, H. Minamiue, H. Inaba, J. Mizusaki, and T. Hashimoto, *Proc. of the 5th International Symposium on Solid Oxide Fuel Cells (SOFC-V)*, (Eds. U. Stimming, S. C. Singhal, H. Tagawa, and W. Lehnert), PV 97-18, 785, The Electrochemical Society Inc., Pennington, NY, USA (1997).